An Experimental Validation of Finite Element Method Versus Data Based Modelling When Applied to the Dynamic Modelling of Spatial Manipulator

H. Sayed[1], A. Abdelhamid[1] and E. M. Shaban[2]

[1]Mechanical Design Department, Faculty of Engineering (Mattaria), Helwan University, Cairo, Egypt.
[2]Faculty of Engineering, Jazan University, – Saudi Arabia, on leave from Faculty of Engineering (Mataria), Helwan University, Cairo, Egypt.
modern3@hotmail.com

Abstract: This paper is concerned with the design and dynamic modelling of four degrees-of-freeedom (DOFs) spatial manipulator with experimental validation which will provide the essential insights to control the system. Two different approaches were employed for dynamic modelling of the system; they are the physical finite element (FE) method and the experimental data-based model (DBM) in discrete time transfer function (TF). A comparison between the two approaches is carried out, in terms of modelling accuracy, along with experimental validation by real time implementation of the manipulator. In the first approach, each link was treated as a finite element and the total displacement was derived by means of the shape function of each element. However, in the second approach, experimental on-line data were used to derive the discrete time TF of each link. The comparison study of the real time implementation suggests that both approaches provide acceptable dynamic modelling for the manipulator in terms of torque exerted by each joint when the end-effector trace a specified path in a given time; however the experimental data-based approach shows acceptable accuracy with straightforward modelling when compared to modelling using FE approach.

Keywords: State Dependent Parameter (SDP), Finite Element Method (FEM), discrete time modelling, dynamics of manipulator arm

1. Introduction

Manipulators have become an indispensable system of many fields, including but not limited to fire fighting, monitoring and inspection, and material handling. Positioning accuracy during maneuvering of the manipulator system is one of the important factors of its geometrical design, dynamic modeling, and control. Therefore it is desirable to design and construct lightweight but rigid manipulators for manufacturing which require robot manipulator to be capable of moving swiftly. At relatively high operational speeds, inertial forces of moving components become quite large, leading to considerable deformation in the lightweight links, and generating unwanted vibration phenomena [1]. Through the previous decades, significant progresses have been made into the dynamic modelling of such manipulators e.g. [1-6]. The finite element approach has been reported for modeling the dynamics of manipulators in several publications, e.g. [1, 7-10]. Experimental or data based modelling (DBM) has been utilized in several applications of robots, e.g. [11-18]. A comparison between the two approaches in terms of accurate dynamic modeling of the manipulator system has not been devoted which will elect the proposed model for the control of motions of the manipulator in order to achieve satisfactory performance.

In this regard, this article aims to developing two dynamical models for 4 DOFs spatial manipulator; they are the physical FE model and the experimental data-based TF model. A consistent comparison between the two models takes place and are benchmarked with a real time implementation of the manipulator when performs a predetermined task.

2. Test Rig: Four DOFs Spatial Manipulator

This section introduces the laboratory four DOFs spatial manipulator, for which four joints have to be synchronisely controlled in order to trace a predetermined trajectory for the end-effector. Here, an open-loop supervisory controller is used to determine the appropriate trajectories for the joints' angles.

As shown in Fig. 1, the manipulator arm is a vertically articulated robot with a slew joint (4) which rotates the whole arm in a horizontal plane and three revolute joints, shoulder (1), elbow (2) and wrist (3) joints which rotate the robot's links in a vertical plane. All joints are actuated by means of geared DC motors with several kinds of transmission which used to operate the links mechanically. To reduce the payload

at joints, all drives are mounted at the robot base to drive the slew and shoulder joints; however the elbow and wrist joints are driven by means of DC motors via timing belts. As shown in Fig. 1, the whole system is supported by multiple I/O asynchronous real-time control system to control the velocity of the joints by means of the applied voltage signal. Subsequently, four transducers are installed in the joints for feedback and to enable closed-loop control of each joint.

1- Shoulder joint   2- Elbow joint
3- Wrist joint   4- Slew joint
5- Laptop   6- Signal conditioning board
7-NI DAQ 6212   8- Labjack UE9 pro
9-Power supply
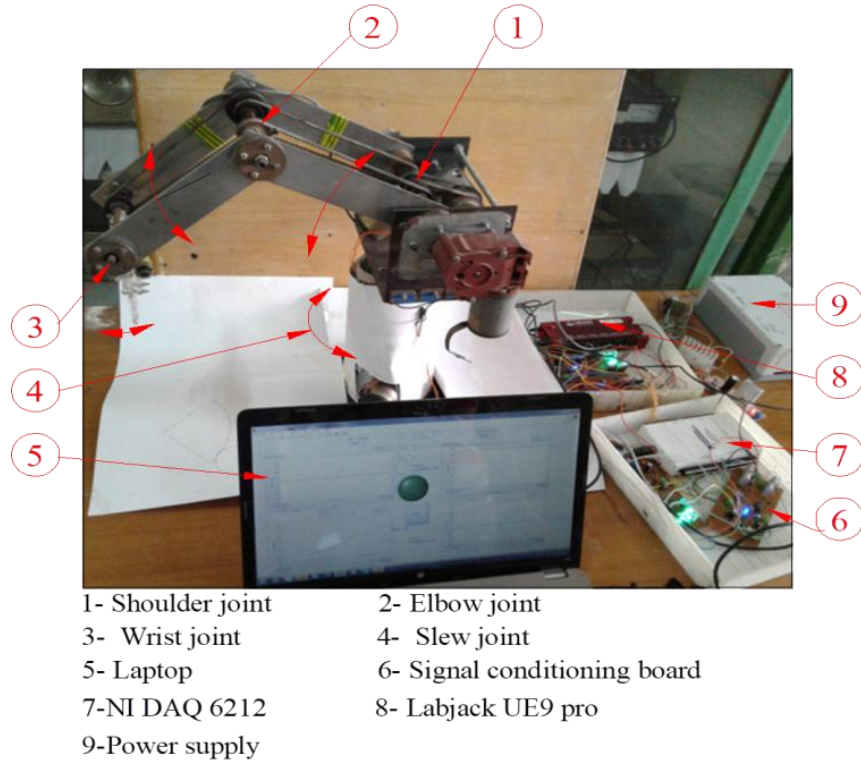
Fig. 1 The manipulator arm with its peripherals.

For the control purpose, it is convenient to mention three key elements of hardware used, they are:

(a) Transducers:

The joints' angles are measured directly by means of rotary potentiometers concentric with each joint pivot. Each potentiometer is a resistive element ($5\,\Omega$ conductivity) with a wiper that divides the voltage source into two divides according to the position of the wiper. Here, an input voltage of 5 volt is used as a source, and the measured analogue voltage is directly connected to the analogue input of the LabJack UE9 and NI DAQ 6212, see Fig. 2.
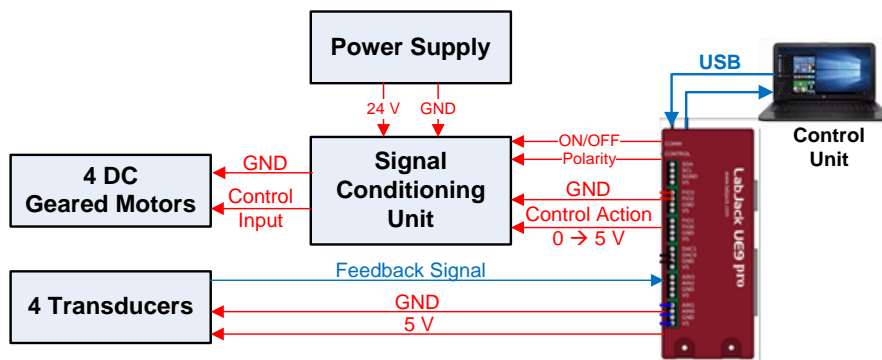
Fig. 2 General layout of laboratory manipulator arm interfacing.

(b) Actuators:

Each joint in the arm manipulator is actuated by DC geared motor. The direction of motor rotation is determined by the polarity of the operating voltage,

also the control unit calculates the required control action which applied to the actuator via the signal conditioning unit. Actuators parameters are summerized in Table 1.

Table 1. Actuators parameters for the laboratory manipulator.

			Slew	Shoulder	Elbow	Wrist
Rotor inertia,	J_m	[g.cm^2]	330	180	180	330
Motor damping constant,	B_m	[kg m^2 s^{-1}]	6.4×10^{-5}	3.4×10^{-5}	3.4×10^{-5}	6.4×10^{-5}
Armature resistance,	R	[Ω]	2.7	4	4	2.7
Torque constant,	K_m	[N.m/amp]	0.047	0.0029	0.0029	0.047
Back emf constant,	K_b	[V.s]	0.10550	0.051341	0.051341	0.10550
Motor speed to joint speed,	r		50	170.5	139	21.4

$d = 385$ mm
$a_2 = 217.5$ mm
$a_3 = 2018$ mm
$a_4 = 150$ mm
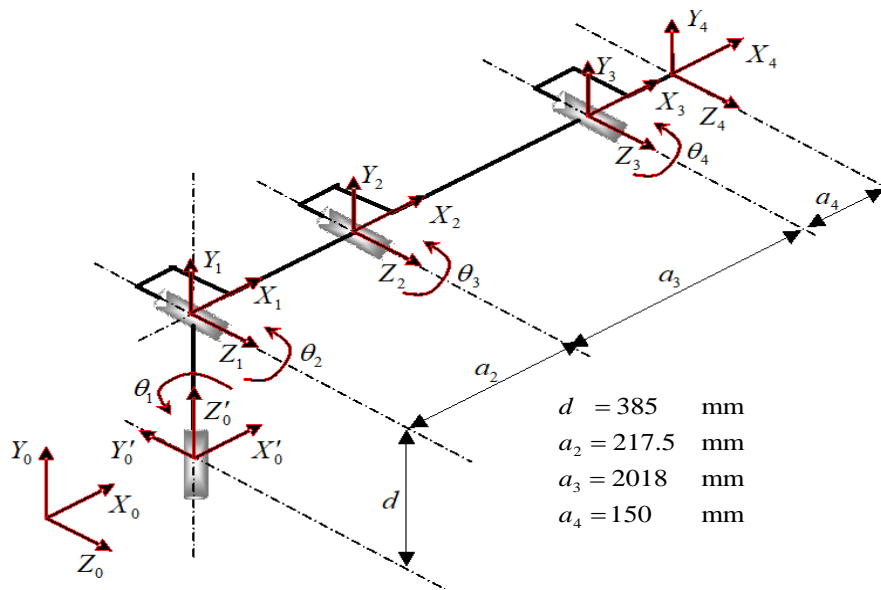
Fig. 3 Schematic diagram showing the coordinate definition for each joint of the manipulator arm.

(c) Data acquisition cards:

Data acquisition boards interface the laptop (control unit) with the hardware prepherals (transducers and actuators), see Fig. 2. The boards are signal conditioning board, NI DAQ 6212, and LabJack UE9 pro, see Fig. 1 and numbered as items 6, 7, and 8 respectively. These boards allow the use of time step 40 ms, i.e. 25 samples/sec, and they are used for interfacing, monitoring and control actions.

3. Kinematics of the Laboratory Manipulator Arm

Fig. 3 demonstrate the laboratory arm with its dimensions, given θ_i (joint angles) where $i = 1, 2, 3$, and 4 for the slew, shoulder, elbow, and wrist respectively, as well as the link lengths $\{d, a_i\}$. Here,

$\{x_i, y_i, z_i\}$ represent the local coordinate systems for the joints, while $\{X_o, Y_o, Z_o\}$ is the global framework originating at the workbench.

Kinematic analysis is typically based on the Denavit-Hartenberg (DH) convention which used for open chain manipulators with joints having one DOF each. Given the following DH parameters:

Joint	θ_i	α_i	a_i	d_i
1	Rotation about X_o by -90°			
	θ_1	90	0	d
2	θ_2	0	a_2	0
3	θ_3	0	a_3	0
4	θ_4	0	a_4	0

for which α_i is the the angle between the z_{i-1}-axis and the z_i-axis about the x_i-axis. Then it is possible to find the position and orientation of the end effector with respect to the reference coordinate system, given the joint variable vectors $\mathbf{\theta}=\begin{bmatrix} \theta_1 & \theta_2 & \theta_3 & \theta_4 \end{bmatrix}^T$ of the arm and the various geometric links parameters as follows:

$$T_0^4 = T_0^1 T_1^2 T_2^3 T_3^4$$

$$= \begin{bmatrix} C_1 C_{234} & -C_1 S_{234} & S_1 & (a_2 C_2 + a_3 C_{23} + a_4 C_{234})C_1 \\ S_{234} & C_{234} & 0 & (a_2 S_2 + a_3 S_{23} + a_4 S_{234}) + d \\ -S_1 C_{234} & S_1 S_{234} & C_1 & -(a_2 C_2 + a_3 C_{23} + a_4 C_{234})S_1 \\ 0 & 0 & 0 & 1 \end{bmatrix} \quad (1)$$

for which C_{ij} and S_{ij} denotes $\cos(\theta_i + \theta_j)$ and $\sin(\theta_i + \theta_j)$ respectively.

4. Finite Element (FE) Modelling

In this section, the physical modelling of the laboratory manipulator takes place by means of finite element method, in which each link in the manipulator is modelled as an element in space. Here, each link with length l has its own specific mass ρ, cross sectional area A, and a moment of inertia I. As showm in Fig. 4, a field point P at a distance ξl, for which ξ is a dimensionless quantity, and has a range $0 \rightarrow 1$, undergoes an absolute displacement in both axial and transverse directions.
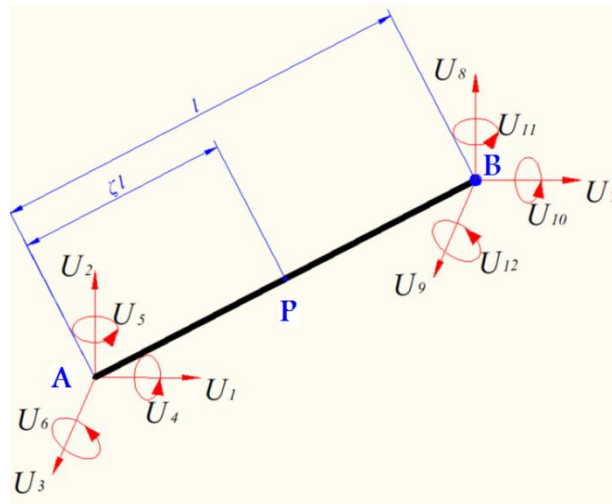
Fig. 4 Rigid body configuration in space of each link element of the manipulator arm.

If we considered an element dm at point P, The kinetic energy for this element is

$$d\left(\mathbf{KE}^e\right) = \frac{1}{2} dm\, \dot{\mathbf{U}}^T \dot{\mathbf{U}} + \frac{1}{2} \mathbf{\omega}^T d\mathbf{I}\, \mathbf{\omega} \quad (2)$$

where $dm = \rho A l\, d\zeta = m\, d\zeta$, $\dot{\mathbf{U}} = \begin{bmatrix} \dot{X} & \dot{Y} & \dot{Z} \end{bmatrix}^T$ is the velocity vector of the centroid of the element dm, $\mathbf{\omega}$ is the angular velocity vector of link AB and $d\mathbf{I}$ is the second moment of inertia for the link element. $\dot{\mathbf{U}}$ can be calculated as

$$\dot{\mathbf{U}} = \mathbf{v_A} + \mathbf{\omega} \times \mathbf{r_{PA}} + \mathbf{v_B} - \mathbf{\omega} \times \mathbf{r_{BP}} \quad (3)$$

where $\mathbf{v_A} = \begin{bmatrix} \dot{U}_1 & \dot{U}_2 & \dot{U}_3 \end{bmatrix}^T$ is the absolute velocity of point A, $\mathbf{v_B} = \begin{bmatrix} \dot{U}_7 & \dot{U}_8 & \dot{U}_9 \end{bmatrix}^T$ is the absolute

velocity of point B, $\mathbf{r_{PA}} = \begin{bmatrix} \zeta l_x & \zeta l_y & \zeta l_z \end{bmatrix}^T$ is the absolute displacement from point A to point P, and $\mathbf{r_{BP}} = \begin{bmatrix} (1-\zeta)l_x & (1-\zeta)l_y & (1-\zeta)l_z \end{bmatrix}^T$ is the absolute displacement from point P to point B. It is convenient to note here that the absolute angular velocity of the link, $\mathbf{\omega}$, equals to $\begin{bmatrix} \dot{U}_4 & \dot{U}_5 & \dot{U}_6 \end{bmatrix}^T = \begin{bmatrix} \dot{U}_{10} & \dot{U}_{11} & \dot{U}_{12} \end{bmatrix}^T$. Given the components of link AB in X, Y, and Z-direction as $l_x = U_7 - U_1$, $l_y = U_8 - U_2$, $l_z = U_9 - U_3$ and substituting in (4), then

$$\dot{\mathbf{U}} = \begin{bmatrix} \dot{U}_1 \\ \dot{U}_2 \\ \dot{U}_3 \end{bmatrix} + \begin{bmatrix} i & j & k \\ \dot{U}_4 & \dot{U}_5 & \dot{U}_6 \\ \zeta l_x & \zeta l_y & \zeta l_z \end{bmatrix} + \begin{bmatrix} \dot{U}_7 \\ \dot{U}_8 \\ \dot{U}_9 \end{bmatrix} - \begin{bmatrix} i & j & k \\ \dot{U}_{10} & \dot{U}_{11} & \dot{U}_{12} \\ (1-\zeta)l_x & (1-\zeta)l_y & (1-\zeta)l_z \end{bmatrix} \quad (4)$$

The above representation of the velocity vector of the element can be written as

$$\dot{\overline{\mathbf{U}}} = \mathbf{N}\dot{\mathbf{U}} \tag{5}$$

where $\dot{\mathbf{U}} = [\dot{U}_1 \;\; .... \;\; \dot{U}_{12}]^T$ is the absolute linear and angular velocities of the link and $\mathbf{N}$ is the shape function for the link element and takes the form,

$$\mathbf{N} = \frac{1}{2}\begin{bmatrix} 1 & 0 & 0 & 0 & \zeta l_z & -\zeta l_y & 1 & 0 & 0 & 0 & (\zeta-1)l_z & (1-\zeta)l_y \\ 0 & 1 & 0 & -\zeta l_z & 0 & \zeta l_x & 0 & 1 & 0 & (1-\zeta)l_z & 0 & (\zeta-1)l_x \\ 0 & 0 & 1 & \zeta l_y & -\zeta l_x & 0 & 0 & 0 & 1 & (\zeta-1)l_y & (1-\zeta)l_x & 0 \end{bmatrix} \tag{6}$$

In the other hand, the term $d\mathbf{I}$ in equation (2) can be represented as

$$\mathbf{KE}^e = \mathbf{KE}^e_{\text{link}} + \mathbf{KE}^e_{\text{payload}}$$

$$= \frac{1}{2}m\int_0^1 \left(\dot{\mathbf{U}}^T \mathbf{N}^T \mathbf{N} \dot{\mathbf{U}}\right)d\xi + \frac{1}{2}\frac{m}{A}\int_0^1 \left[\dot{U}_4 \;\; \dot{U}_5 \;\; \dot{U}_6\right]\mathbf{R}\,\overline{\mathbf{D}}_{\mathbf{A}}\,\mathbf{R}^T \begin{bmatrix} \dot{U}_4 \\ \dot{U}_5 \\ \dot{U}_6 \end{bmatrix} d\zeta + \frac{1}{2}\dot{\mathbf{U}}^T\,\mathbf{M}^e_p\,\dot{\mathbf{U}} \tag{9}$$

Then

$$\mathbf{KE}^e = \frac{1}{2}\dot{\mathbf{U}}^T \overline{\mathbf{M}}^e \dot{\mathbf{U}} + \frac{1}{2}\dot{\mathbf{U}}^T \overline{\overline{\mathbf{M}}}^e \dot{\mathbf{U}} + \frac{1}{2}\dot{\mathbf{U}}^T \mathbf{M}^e_p \dot{\mathbf{U}}$$

$$= \frac{1}{2}\dot{\mathbf{U}}^T \left(\overline{\mathbf{M}}^e + \overline{\overline{\mathbf{M}}}^e + \mathbf{M}^e_p\right)\dot{\mathbf{U}} \tag{10}$$

$$= \frac{1}{2}\dot{\mathbf{U}}^T \mathbf{M}^e \dot{\mathbf{U}}$$

where the elemental mass matrix $\mathbf{M}^e$ is the sum of the following matrices

$$\overline{\mathbf{M}}^e = m\int_0^1 \mathbf{N}^T \mathbf{N}\, d\xi \,,$$

$$\overline{\overline{\mathbf{M}}}^e = \frac{m}{A}\begin{bmatrix} \mathbf{0}_{3\times3} & \mathbf{0}_{3\times3} & \mathbf{0}_{3\times6} \\ \mathbf{0}_{3\times3} & \mathbf{R}\,\overline{\mathbf{D}}_{\mathbf{A}}\mathbf{R}^T & \mathbf{0}_{3\times6} \\ \mathbf{0}_{6\times3} & \mathbf{0}_{6\times3} & \mathbf{0}_{6\times6} \end{bmatrix},$$

$$\mathbf{M}^e_p = m_p \left[\begin{array}{c|c} \underset{6\times6}{\mathbf{0}} & \underset{6\times6}{\mathbf{0}} \\ \hline \underset{6\times6}{\mathbf{0}} & \begin{array}{cc} \underset{3\times3}{\mathbf{I}} & \mathbf{0} \\ \mathbf{0} & \underset{3\times3}{\mathbf{0}} \end{array} \end{array}\right], \text{ and}$$

Here, m_p is the payload at the end of the link element.

The expression for $\overline{\mathbf{M}}^e$ is defined in the appendices.

An expression for the dynamic behaviour of the link element can be achieved by means of the Lagrange's equation

$$\frac{d}{dt}\left(\frac{\partial}{\partial \dot{\mathbf{U}}}\mathbf{KE}^e\right) - \frac{\partial}{\partial \mathbf{U}}\mathbf{KE}^e = \mathbf{Q}^e \tag{11}$$

$$d\mathbf{I} = \mathbf{R}\,d\overline{\mathbf{D}}\,\mathbf{R}^T \tag{7}$$

where $\mathbf{R}$ is the rotation matrix of the element dm and $d\overline{\mathbf{D}}$ is its local inertia tensor. Given that the element length $l\,d\zeta$ is very small then

$$d\overline{\mathbf{D}} = \rho\,l\,d\left(\zeta\,\overline{\mathbf{D}}_{\mathbf{A}}\right) = \frac{m}{A}\,d\left(\zeta\,\overline{\mathbf{D}}_{\mathbf{A}}\right) \tag{8}$$

where $\overline{\mathbf{D}}_{\mathbf{A}}$ is the second moment of area tensor in local coordinates. Substituting into equation (2), the kinetic energy of the link can be calculated, including the payload, as follows:

for which the term $\mathbf{Q}^e$ is related to the generalized external forces. Given the kinetic energy $\mathbf{KE}^e$ in (10) and substituting in (11), the individual elemental equation of motion for each link can be derived and takes the form

$$\mathbf{M}^e\,\ddot{\mathbf{U}} + \mathbf{C}^e\,\dot{\mathbf{U}} + \mathbf{H}^e\,\mathbf{U} = \overline{\mathbf{Q}}^e \tag{12}$$

for which $\mathbf{C}^e = \dot{\mathbf{M}}^e$ and $\mathbf{H}^e\mathbf{U} = -\partial \mathbf{KE}^e/\partial \mathbf{U}$. A full expression for the elemental gyroscopic and centripetal matrices $\mathbf{C}^e$ and $\mathbf{H}^e$ are defined in the appendices. The vector $\overline{\mathbf{Q}}^e$ represents the external forces neglecting surface traction and joint friction. This generalized force vector can be split into gravitational $\mathbf{Q}_g = \mathbf{M}^e\mathbf{g}$ and applied loading $\mathbf{Q}$, if any.
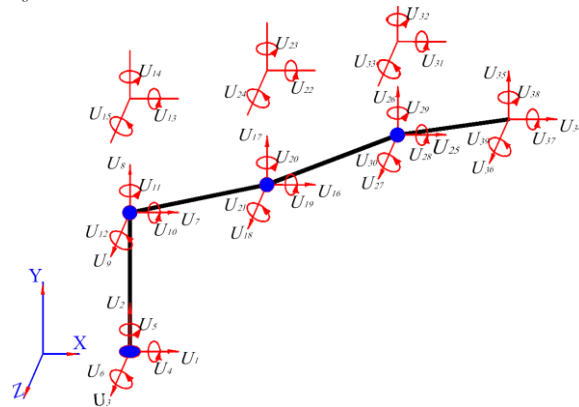
Fig. 5 The nodal displacement configuration of the manipulator arm

In the case of 4-axes articulated manipulator under study, the four links are moving in the X-Y-Z plane, as shown in Fig. 5, for which each individual link is considered as an elements.

The elemental mass matrices, gyroscopic matrices and centripetal matrices can be assembled together to obtain the 39×39 global system mass, gyroscopic and centripetal matrices $\{\mathbf{M}, \mathbf{C}, \mathbf{H}\}$ for the whole manipulator. The definition of these global matrices can then be used to form the global system equation of motion which may take the following form

$$\begin{bmatrix} T_{M_1} \\ T_{M_2} \\ T_{M_3} \\ T_{M_4} \end{bmatrix} = \mathbf{J}_4^T \begin{bmatrix} Q_{34} \\ Q_{35} \\ Q_{36} \\ Q_{37} \\ Q_{38} \\ Q_{39} \end{bmatrix} + \mathbf{J}_{\omega_4}^T \begin{bmatrix} Q_{31} \\ Q_{32} \\ Q_{33} \end{bmatrix} + \mathbf{J}_3^T \begin{bmatrix} Q_{25} \\ Q_{26} \\ Q_{27} \\ Q_{28} \\ Q_{29} \\ Q_{30} \end{bmatrix} + \mathbf{J}_{\omega_3}^T \begin{bmatrix} Q_{22} \\ Q_{23} \\ Q_{24} \end{bmatrix} + \mathbf{J}_2^T \begin{bmatrix} Q_{16} \\ Q_{17} \\ Q_{18} \\ Q_{19} \\ Q_{20} \\ Q_{21} \end{bmatrix} + \mathbf{J}_{\omega_2}^T \begin{bmatrix} Q_{13} \\ Q_{14} \\ Q_{15} \end{bmatrix} + \mathbf{J}_1^T \begin{bmatrix} Q_7 \\ Q_8 \\ Q_9 \\ Q_{10} \\ Q_{11} \\ Q_{12} \end{bmatrix} + \mathbf{J}_{\omega_1}^T \begin{bmatrix} Q_4 \\ Q_5 \\ Q_6 \end{bmatrix} \qquad (14)$$

where $\mathbf{J}_i$ and $\mathbf{J}_{\omega_i}$ for $(i = 1, ..., 4)$ are the Jacobian matrix and the rotation Jacobian matrix for link i.

The second moment of area tensor $\bar{\mathbf{D}}_A$ for each link, existed in equations (8, 9 and 10), is difficult to be obtained due to the irregularity and nonhomogeneity existed in the manipulator links. However, it is possible to use dynamic equivalence [19] to convert any nonhomogeneous link into

$$\mathbf{M}\,\ddot{\mathbf{U}} + \mathbf{C}\,\dot{\mathbf{U}} + \mathbf{H}\,\mathbf{U} = \bar{\mathbf{Q}} \qquad (13)$$

for which $\bar{\mathbf{Q}} = \mathbf{Q}_g + \mathbf{Q}$, recalling that $\mathbf{Q}_g = \mathbf{M}\mathbf{g}$ is the gravitational force for the whole manipulator, given that $\mathbf{g} = -g \begin{bmatrix} 0 & 1 & 0_{1\times5} & 1 & 0_{1\times8} & 1 & 0_{1\times8} & 1 & 0_{1\times8} & 1 & 0_{1\times4} \end{bmatrix}^T$, and $\mathbf{Q} = \begin{bmatrix} Q_1 & \cdots & Q_{39} \end{bmatrix}^T$ is the applied loading vector. The required torque at each joint can then be calculated as follows:

homogeneous link with constant ρA, see Fig. 6. As shown in this figure, the nonhomogeneous link, with length l, mass m, and mass moment of inertia about its local coordinates $\{I_x, I_y, I_z\}$, is converted to homogeneous link with mass m_l and two concentric masses at its ends m_{P_0} and m_{P_1}. Dynamic equivalence is listed with discussion in the Appendices.
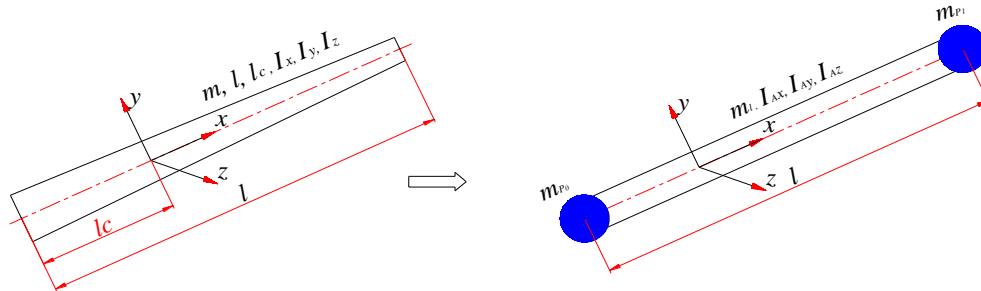
Fig. 6 The dynamic equivalence for nonhomogeneous link.

Now, the second moment of area tensor in local coordinates for homogeneous link can be defined as

$$\frac{m_l}{A} \bar{\mathbf{D}}_A = \begin{bmatrix} I_{Ax} & 0 & 0 \\ 0 & I_{Ay} & 0 \\ 0 & 0 & I_{Az} \end{bmatrix} \qquad (15)$$

for which I_{Ax}, I_{Ay}, and I_{Az} depend upon the cross sectional area of the link not its length.

5. Experimental Data Based Modelling

Experimental data based modelling (DBM) is the development of mathematical models of dynamic systems on the basis of measured on-line data from experiments. Here, the data are collected and utilized in identifying the structure of the dynamic model, i.e. the orders of the polynomials in the transfer function (TF) and the pure time delay, and to estimate the discrete time TF parameters which characterizes the dynamics of the system [20, 21]. Sophisticated time-

series methods which employ the simplified refined instrumental variable (SRIV) are developed for parameter estimates [22-24]. These statistical tools and associated estimation algorithms have been assembled in the Matlab® software as the CAPTAIN toolbox [25]. The representation of dynamical systems using State Dependent Parameter TF (SDP-TF) models can be traced to earlier publications such as [26]. In this paper, an SDP-TF model, written in discrete-time incremental form, is considered as

$$y_k = -a_1(\chi_k)y_{k-1} - \cdots - a_n(\chi_k)y_{k-n} + b_1(\chi_k)u_{k-1} + \cdots + b_m(\chi_k)u_{k-m} \tag{16}$$

where u_k and y_k are the input and output variables respectively. The parameters $a_i(\chi_k)$ $\forall 1 \le i \le n$ and $b_j(\chi_k)$ $\forall 1 \le j \le m$ are themselves functions of the lagged system variables. In TF form, the model (16) becomes,

$$y_k = \frac{b_{1,k+1}z^{-1} + \cdots + b_{m,k+m}z^{-m}}{1 + a_{1,k+1}z^{-1} + \cdots + a_{n,k+n}z^{-n}}u_k$$
$$= \frac{B_k(z^{-1})}{A_k(z^{-1})}u_k \tag{17}$$

where z^{-1} is the backward shift operator, for which $z^{-i}y(k) = y(k-i)$. SDP-TF model (17) alludes to the time variable parameter derivation of the SDP model, see [24] for details. The backward shift operator notation utilized in (17) suggests that, for example, if $a_{1,k} = a_1(\chi_k) = f(y_{k-1})$ then $a_{1,k+1} = a_1(\chi_{k+1})$ is a function of the un-lagged output y_k.

The first step is defining the appropriate structure for the transfer function (17), i.e. the triad $\{n, m, \delta\}$ where δ is the pure time delay, typically represented by setting $b_1 \cdots b_{\delta-1} = 0$. The two main statistical measures employed to help determine these values are the coefficient of determination R_T^2, based on the

response error, which is a simple measure of model fit; and the Young Identification Criterion (YIC), which provides a combined measure of fit and parametric efficiency [22].

In this work, the experimental modelling is carried out using sample rate equals to 25 samples per second, i.e. the time step $\Delta t = 0.04$ sec, for all joints. Pseudo Random Binary Signal (PRBS) input is applied to all joints simultaneously for modelling purpose. Fig. 7 shows the simulation fit of the SDP model of the Slew joint applied to a range of operating levels, where $R_T^2 = 0.87$. Table 2 shows the nonlinear SDP-TF and the linear TF models for the four joints of the manipulator. Here, y_k represents the joint angle in degrees and u_k represents the normalized input.
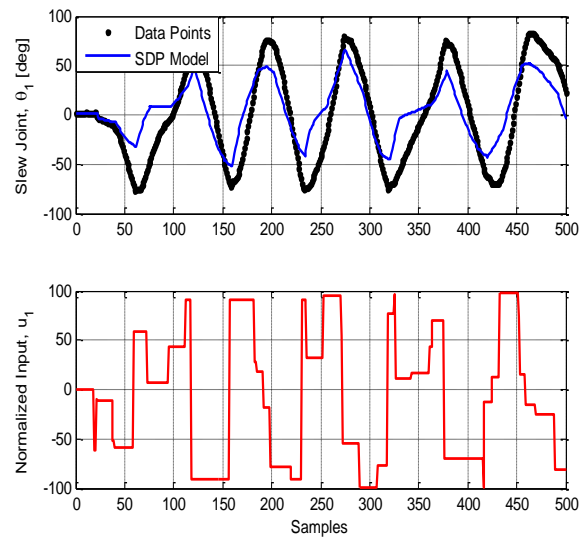
Fig. 7 The open loop experiment (dots) for joint 1 and the model fit for the estimated nonlinear SDP (solid). The normalized PRBS input is shown in the lower plot.

Table 2. The nonlinear SDP and the linear TF models for the four joints of the manipulator

Joint		Model	R_T^2
(1) Slew	Linear	$y_k = 1.808 y_{k-1} - 0.808 y_{k-2} + 0.0107 u_{k-1}$	0.83
	Nonlinear	$y_k = -(2.9 \times 10^{-7} u_{k-1}^2 - 1.81)y_{k-1} - (1.9 \times 10^{-6} u_{k-1} + 0.81)y_{k-2}$ $+ (-5.18 \times 10^{-7} u_{k-1}^2 + 0.0152)u_{k-1}$	0.87
(2) Shoulder	Linear	$y_k = 0.995 y_{k-1} + 0.0335 u_{k-4}$	0.64
	Nonlinear	$y_k = -(3.653 \times 10^{-4} y_{k-1} - 0.97)y_{k-1} + 0.0386 u_{k-4}$	0.82

(3) Elbow	Linear	$y_k = 1.6042\, y_{k-1} - 0.6046\, y_{k-2} + 0.0209\, u_{k-1}$	0.81
	Nonlinear	$y_k = -\left(2.0366\times10^{-5} u_{k-2} - 1.72\right) y_{k-1} - \left(-9.08\times10^{-7} y_{k-1}^{2} + 0.73\right) y_{k-2}$ $+ \left(1.88\times10^{-7} u_{k-2}^{2} + 0.0144\right) u_{k-2}$	0.90
(4) wrist	Linear	$y_k = 1.7726\, y_{k-1} - 0.7735\, y_{k-2} + 0.0365\, u_{k-1}$	0.82
	Nonlinear	$y_k = -\left(1.779\times10^{-6} u_{k-1}^{2} - 1.775\right) y_{k-1} + \left(1.717\times10^{-6} u_{k-1}^{2} - 0.7776\right) y_{k-2}$ $+ \left(7.163\times10^{-5} u_{k-1} + 0.0485\right) u_{k-1}$	0.85

6. Application to the Manipulator Arm

This section is concerned with the real time application of both approaches; physical FEM and the experimental DBM, when both applied in discrete time. A comparison between the two approaches is carried out, in terms of modelling accuracy, i.e. the normalized input exerted by each joint, when the manipulator moves randomely from point-to-point. The normalized inputs required for the four joints of the manipulator arm to accomplish the path of the end effector are calculated by using both approaches and

compared to the real time inputs (torques) exerted by the same joints of the manipulator.

In this regard, inputs are given to the four joints of the manipulator arm to move its end-effector from a point $\{0.3, 0.02, 0\}$ with an orientation to the vertical plan $\Theta = -87.5^{\circ}$ to another point $\{0, 0.73, 0.35\}$ with an orientation to the vertical plan $\Theta = -4^{\circ}$ in 3.2 seconds, i.e. 80 samples. Fig. (8) shows the joints' trajectory of the manipulator arm during the experiment, however Fig. (9) shows the corresponding end-effector position in global coordinates $\{X, Y, Z\}$.
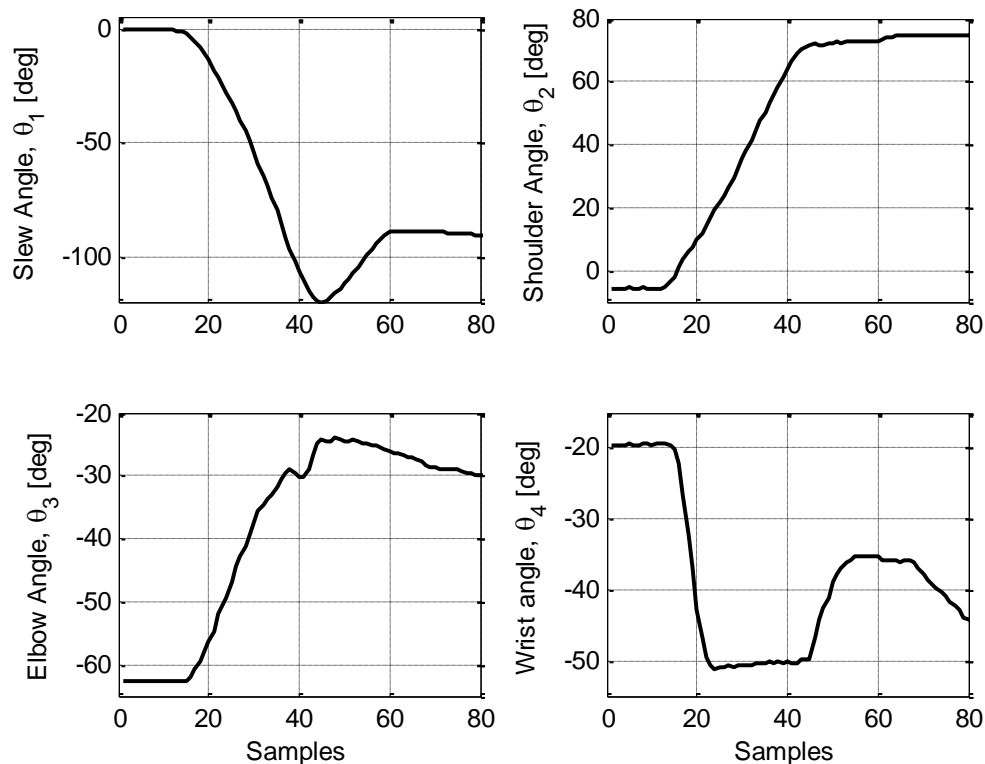
Fig. 8 The joints' trajectory of the manipulator arm during the experiment.
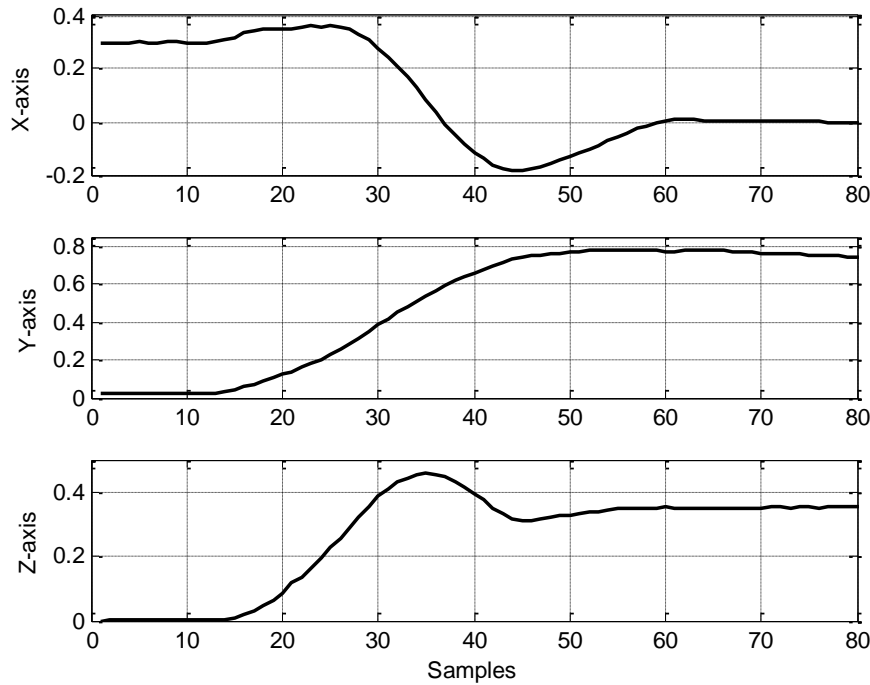
Fig. 9 The global coordinates of the manipulator arm during the experiment $\{X, Y, Z\}$.

In FE approach, the input is the motor voltage V_m, which can be calculated using the following equation [27],

$$J_m r \ddot{\theta}_m(t) + (B_m + K_b K_m / R) r \dot{\theta}_m(t) + T_m(t) = (Km / R) r V_m(t) \quad (18)$$

where the parameters $\{J_m, B_m, K_b, K_m, R, r\}$ are depicted in Table (1) for each motor. Giving that the angular position of each motor is $\theta_m(t) = q(t) r$, where $q(t)$ is the angular position of the driven link, the input voltage of each motor can be computed as

$$V_m(t) = \frac{J_m r^2 \ddot{q}(t) + (B_m + K_b K_m / R) r^2 \dot{q}(t) + T_m(t)}{(K_m / R) r} \quad (19)$$

It is convenient to note that $q_1 = \theta_1$, $q_2 = \theta_2$, $q_3 = \theta_2 + \theta_3$ and $q_4 = \theta_2 + \theta_3 + \theta_4$ for links 1, 2, 3 and 4 respectively.

Given the path in Fig. 9, it is now possible to calculate the torque exerted in each joint, with the aid of the following data for the manipulator arm:

$d = 0.385$ m , $a_2 = 0.2175$ m , $a_3 = 0.208$ m ,

$a_4 = 0.15$ m , $a_{c2} = 0.0904$ m , $a_{c3} = 0.0985$ m ,

$a_{c4} = 0.0235$ m

$m_1 = 6.8$ kg , $m_2 = 1.47$ kg , $m_3 = 1.29$ kg ,

$m_4 = 0.234$ kg , $m_p = 0.5$ kg ,

$I_{1y} = 0.067439$ kg.m^2 , $I_{2x} = 9.932 \times 10^{-3}$ kg.m^2 ,

$I_{2y} = 2.1628 \times 10^{-2}$ kg.m^2 , $I_{2z} = 1.2048 \times 10^{-2}$ kg.m^2 ,

$I_{3x} = 7.2274 \times 10^{-3}$ kg.m^2 , $I_{3y} = 1.7927 \times 10^{-2}$ kg.m^2

$I_{3z} = 1.1046 \times 10^{-2}$ kg.m^2 , $I_{4x} = 3.5381 \times 10^{-4}$ kg.m^2 ,

$I_{4y} = 7.0213 \times 10^{-4}$ kg.m^2 , $I_{4z} = 3.5836 \times 10^{-4}$ kg.m^2

In order to calculate the matrices $\mathbf{M^e}$, $\mathbf{C^e}$ and $\mathbf{H^e}$, it is required to determinre the set of parameters $\{l_x, l_y, l_z, v_x, v_y, v_z, \dot{U}_4, \dot{U}_5, \dot{U}_6\}$ for each link as follows,

Link 1	$l_x = 0$,	$l_y = 0$,	$l_z = 0$
	$\dot{U}_4 = \omega_x = 0$,	$\dot{U}_5 = \omega_y = \omega_1$,	$\dot{U}_6 = \omega_z = 0$
	$v_x = \dfrac{dl_x}{dt} = 0$,	$v_y = \dfrac{dl_y}{dt} = 0$,	$v_z = \dfrac{dl_z}{dt} = 0$
Link 2	$l_x = a_2 C_1 C_2$,	$l_y = a_2 S_2$,	$l_z = -a_2 S_1 C_2$
	$\dot{U}_4 = \omega_2 S_1$,	$\dot{U}_5 = \omega_1$,	$\dot{U}_6 = \omega_2 C_1$
	$v_x = -a_2 S_1 C_2 \omega_1 - a_2 C_1 S_2 \omega_2$,		
	$v_y = a_2 C_2 \omega_2$,		
	$v_z = a_2 S_1 S_2 \omega_2 - a_2 C_1 C_2 \omega_1$		

Link 3	$l_x = a_3C_1C_{23}, \qquad l_y = a_3S_{23}, \qquad l_z = -a_3S_1C_{23}$ $\dot{U}_4 = (\omega_2 + \omega_3)S_1, \ \dot{U}_5 = \omega_1, \qquad \dot{U}_6 = (\omega_2 + \omega_3)C_1$ $v_x = -a_3S_1C_{23}\omega_1 - a_3C_1S_{23}(\omega_2 + \omega_3),$ $v_y = a_3C_{23}(\omega_2 + \omega_3),$ $v_z = a_3S_1S_{23}(\omega_2 + \omega_3) - a_3C_1C_{23}\omega_1$
Link 4	$l_x = a_4C_1C_{234}, \qquad l_y = a_4S_{234}, \qquad l_z = -a_4S_1C_{234}$ $\dot{U}_4 = (\omega_2 + \omega_3 + \omega_4)S_1, \qquad \dot{U}_5 = \omega_1,$ $\dot{U}_6 = (\omega_2 + \omega_3 + \omega_4)C_1$ $v_x = -a_4S_1C_{234}\omega_1 - a_4C_1S_{234}(\omega_2 + \omega_3 + \omega_4)\omega_2,$ $v_y = a_4C_{234}(\omega_2 + \omega_3 + \omega_4),$ $v_z = a_4S_1S_{234}(\omega_2 + \omega_3 + \omega_4) - a_4C_1C_{234}\omega_1$

It is convenient to note here that the torque exerted in each joint is then normalized in the range −100 to 100 for the sake of comparison.

In data based modelling, straightforward algebra can be used to calculate the normalized input u_k by inversing the TF of each joint tabulated in Table (2), giving the link angle y_k.

The normalized input of each joint in the manipulator arm can be then calculated by using both physical FEM and experimental DBM. The results are plotted in Fig. 10 which shows little difference between both approaches when compared to the real normalized inputs given to the joints. The same figure suggest the use of DBM, since it gives closer inputs when compared to the real inputs especially for slew, shoulder and elbow joints. The fourth joint, wrist, may need extra effort for modelling.

7. Conclusions

This paper has developed two different approaches for dynamic modelling of the manipulator arm; they are the physical FEM and the experimental on-line DBM in discrete time. A comparison between the two approaches is carried out, in terms of modelling accuracy, along with experimental validation by real time implementation of the manipulator. The comparison study of the real time implementation suggests that both approaches provide acceptable modelling for the manipulator in terms of torque exerted in each joint; however DBM shows closer results to the real inputs with straightforward modelling when compared to modelling using FEM.
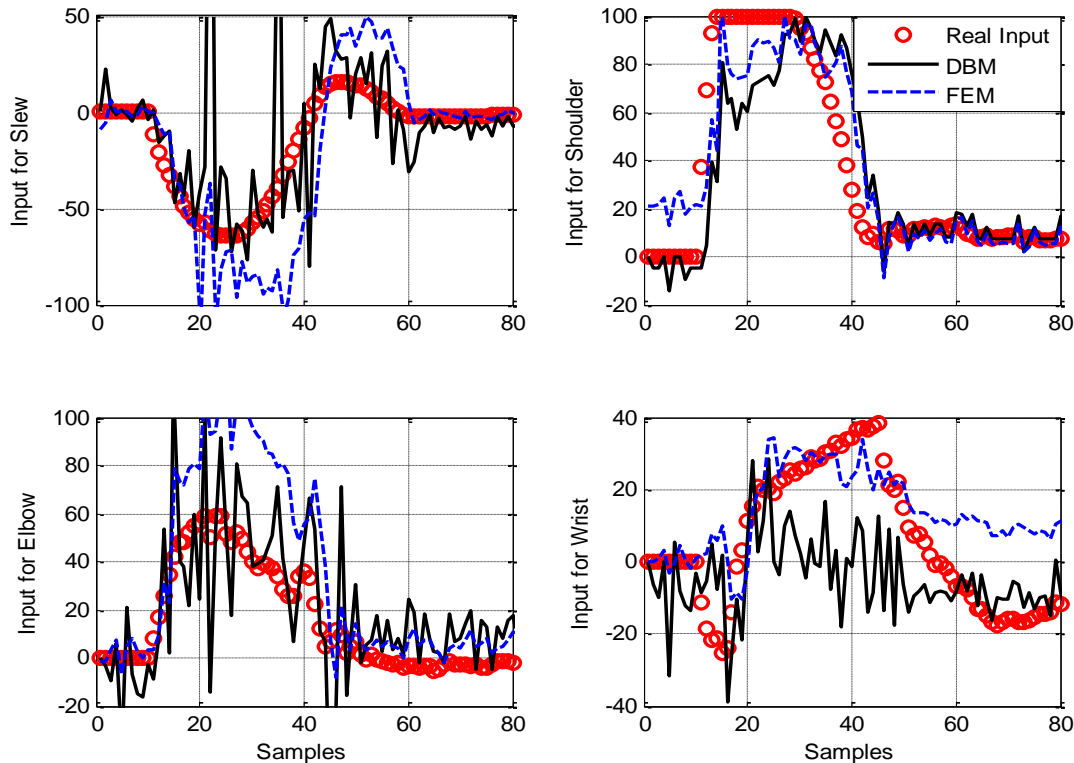
Fig. 10 Comparison between the required normalized input by FEM and DBM when the manipulator arm achieves an arbitrary path shown in Figs. (8 and 9).

References
1. Frederik Foldager, Dan Thomsen, Haijie Li, Kasper Frederiksen, Anders Andersen, Xuping Zhang (2015). Electrical-Mechanical Dynamic Modelling and Testing of a Lightweight-Link Robot Manipulator, In: Proceedings of the World Congress on Mechanical, Chemical, and Material Engineering (MCM 2015), Barcelona, Spain, July 20–21, 2015, Paper No. 251.
2. Lowen, G. G., & Jandrasits, W. G. (1972). Survey Of Investigations Into The Dynamic Behavior Of Mechanisms Containing Links With Distributed Mass And Elasticity. Mechanism and Machine Theory, 7: 3–17.
3. Shabana, A.A. (1997). Flexible Multibody Dynamics: Review of Past and Recent Developments. Multibody System Dynamics. 1: 189–222.
4. Dwivedy, S. K., & Eberhard, P. (2006). Dynamic Analysis of Flexible Manipulators, a Literature Review. Mechanism and Machine Theory. 41: 749–777.
5. Book, W. (1993). Controlled Motion In An Elastic World. ASME Journal of Dynamic Systems, Measurement, and Control. 115: 252–260.
6. Benosman, M., & Vey, G. L. (2004). Control of Flexible Manipulators: A Survey. Robotica. 22: 533–545.
7. Zhang, X., & Yu, Y. (2009). A New Spatial Rotor Beam Element for Modeling Spatial Manipulators with Moint and Link Flexibility. Mechanism and Machine Theory. 35(3): 403–42.
8. Usoro, P. B., Nadira, R., & Mahil, S. S. (1986). A Finite Element/Lagrangian Approach to Modelling Lightweight Flexible Manipulators. ASME Journal of Dynamic Systems, Measurements, and Control. 108: 198–205.
9. Mostafa Sayahkarajy1,2, Z Mohamed1 and Ahmad Athif Mohd Faudzi (2016). Review of modelling and control of flexible-link manipulators. Proc IMechE Part I: J Systems and Control Engineering, 1–13.
10. Lee JD and Ben-Li W. Dynamic equations for a two-link flexible robot arm. Comput Struct 1988. 29(3): 469–477.
11. Shaban, E.M., Ako, S., Taylor, C.J. Seward, D.W., 2008. "Development of an automated verticality alignment system for a vibro-lance". Automation in Construction, 17(5), p. 645–655.
12. Taylor, C.J., Shaban, E.M., Stables, M.A., Ako, S., 2007. "Proportional-Integral-Plus control applications of state dependent parameter models". Journal of System and Control Engineering, 221(7), p. 1019–1031.
13. Sidiropoulou, E., Shaban, E.M., Taylor, C.J., Tych, W., Chotai, A., 2006. "Linear, nonlinear, and classical control of 1/5th scale automated excavator". 18th International Conference on System Engineering, ICSE-06, Convey, UK.
14. Dixon, R., Taylor, C.J., Shaban, E.M., (2005). "Comparison of classical and modern control applied to an excavator arm". International Federation of Automatic Control, 16th Triennial World Congress (IFAC-05), 16(1), p. 1367–1372, Prague, Czech Republic.
15. A. Abdelhamid, E.M. Shaban, K.M. Zied, Younes Khalil, (2013), "Implementation of a Class of True Digital Control (TDC) in the Navigation of a Ground Vehicle", American Journal of Research Communication, Vol. 1 (6), pp. 99 – 111, ISSN: 2325-4076, www.usa-journals.com.
16. E.M. Shaban, and Ayman A. Nada, (2013),"Proportional-Integral-Derivative versus Proportional-Integral-Plus Control Applied to Mobile Robotic System", journal of American Science, http://www.jofamericanscience.org, Vol. 9(12), pp. 583–591.
17. E.M. Shaban, and Ayman A. Nada, (2014), "On linearization of nonlinear dynamic systems described by State Dependent Parameter (SDP) discrete-time model", ECCOMAS 2014, July, Barcelona, Spain.
18. E.M. Shaban, Ayman A. Nada, and C.J. Taylor, (2014), "Exact linearization by feedback of state dependent parameter models applied to a mechatronics demonstrator", UKACC 10th international conference on control, Loughborough University, 9th –11th July 2014, UK.
19. R. L. Norton, (1992), "Design of machinery: An introduction to the synthesis and analysis of mechanisms and machines", New York, McGraw-Hill.
20. P.C. Young, Recursive Estimation and Time Series Analysis, Springer-Verlag, Berlin, 1984.
21. P.C. Young, The instrumental Variable Method: A Practical Approach to Identification and System Parameter Estimation, Appears in H.A. Barker and P.C. Young (ed.), Identification and System Parameter Estimation, Pergamon, Oxford, Vols.1 and 2, pp.1–16, 1985.
22. P.C. Young, "Simplified Refined Instrumental Variable (SRIV) Estimation and True Digital Control (TDC)", 1st European Control Conference, pp.1295–1306 (Grenoble), 1991.
23. P.C. Young, "Data-Based Mechanistic Modelling of Engineering Systems", Journal of Vibration and Control, Vol.4, pp.5–28, 1998.

24. Taylor, C.J., Pedregal, D.J., Young, P.C. and Tych, W. (2007) Environmental Time Series Analysis and Forecasting with the Captain Toolbox, *Environmental Modelling and Software*, 22, pp. 797–814.

25. Young, P.C., Taylor, C.J., Tych, W., Pedregal, D.J. (2007) The Captain Toolbox. Center for Research on Environmental Systems and Statistics, Lancaster University, UK. Internet: www.es.lancs.ac.uk/cres/captain.

26. Young P.C. Stochastic, dynamic modelling and signal processing: time variable and state dependent parameter estimation. Appears in Nonlinear and nonstationary signal processing, W.J. Fitzgerald et al. (Ed.), Cambridge University Press, 74-114, 2000.

27. Spong, M. W., Hutchinson, S., & Vidyasagar, M. (2006). Robot modeling and control. Hoboken, NJ: John Wiley & Sons.

Appendices

(a) The expression for $\bar{\mathbf{M}}^e$

$$\bar{\mathbf{M}}^e = m\int_0^1 \mathbf{N}^T \mathbf{N}\, d\xi$$

$$= \frac{m}{4}\int_0^1 \begin{bmatrix} 1 & 0 & 0 & 0 & \xi l_z & -\xi l_y & 1 & 0 & 0 & 0 & (\xi-1)l_z & (1-\xi)l_y \\ 0 & 1 & 0 & -\xi l_z & 0 & \xi l_x & 0 & 1 & 0 & (1-\xi)l_z & 0 & (\xi-1)l_x \\ 0 & 0 & 1 & \xi l_y & -\xi l_x & 0 & 0 & 0 & 1 & (\xi-1)l_y & (1-\xi)l_x & 0 \end{bmatrix}^T$$
$$\begin{bmatrix} 1 & 0 & 0 & 0 & \xi l_z & -\xi l_y & 1 & 0 & 0 & 0 & (\xi-1)l_z & (1-\xi)l_y \\ 0 & 1 & 0 & -\xi l_z & 0 & \xi l_x & 0 & 1 & 0 & (1-\xi)l_z & 0 & (\xi-1)l_x \\ 0 & 0 & 1 & \xi l_y & -\xi l_x & 0 & 0 & 0 & 1 & (\xi-1)l_y & (1-\xi)l_x & 0 \end{bmatrix} d\xi$$

$$\bar{\mathbf{M}}^e = \frac{m}{24}\begin{bmatrix}
6 & 0 & 0 & 0 & 3l_z & -3l_y & 6 & 0 & 0 & 0 & -3l_z & 3l_y \\
0 & 6 & 0 & -3l_z & 0 & 3l_x & 0 & 6 & 0 & 3l_z & 0 & -3l_x \\
0 & 0 & 6 & 3l_y & -3l_x & 0 & 0 & 0 & 6 & -3l_y & 3l_x & 0 \\
0 & -3l_z & 3l_y & 2(l_y^2+l_z^2) & -2l_xl_y & -2l_xl_z & 0 & -3l_z & 3l_y & -(l_y^2+l_z^2) & l_xl_y & l_xl_z \\
3l_z & 0 & -3l_x & -2l_xl_y & 2(l_x^2+l_z^2) & -2l_yl_z & 3l_z & 0 & -3l_x & l_xl_y & -(l_x^2+l_z^2) & l_yl_z \\
-3l_y & 3l_x & 0 & -2l_xl_z & -2l_yl_z & 2(l_x^2+l_y^2) & -3l_y & 3l_x & 0 & l_xl_z & l_yl_z & -(l_x^2+l_y^2) \\
6 & 0 & 0 & 0 & 3l_z & -3l_y & 6 & 0 & 0 & 0 & -3l_z & 3l_y \\
0 & 6 & 0 & -3l_z & 0 & 3l_x & 0 & 6 & 0 & 3l_z & 0 & -3l_x \\
0 & 0 & 6 & 3l_y & -3l_x & 0 & 0 & 0 & 6 & -3l_y & 3l_x & 0 \\
0 & 3l_z & -3l_y & -(l_y^2+l_z^2) & l_xl_y & l_xl_z & 0 & 3l_z & -3l_y & 2(l_y^2+l_z^2) & -2l_xl_y & -2l_xl_z \\
-3l_z & 0 & 3l_x & l_xl_y & -(l_x^2+l_z^2) & l_yl_z & -3l_z & 0 & 3l_x & -2l_xl_y & 2(l_x^2+l_z^2) & -2l_yl_z \\
3l_y & -3l_x & 0 & l_xl_z & l_yl_z & -(l_x^2+l_y^2) & 3l_y & -3l_x & 0 & -2l_xl_z & -2l_yl_z & 2(l_x^2+l_y^2)
\end{bmatrix}$$

(b) The expression for $\mathbf{C}^e$

$$\dot{\mathbf{M}}^e = \begin{bmatrix}
0 & 0 & 0 & 0 & 3v_z & -3v_y & 0 & 0 & 0 & 0 & -3v_z & 3v_y \\
0 & 0 & 0 & -3v_z & 0 & 3v_x & 0 & 0 & 0 & 3v_z & 0 & -3v_x \\
0 & 0 & 0 & 3v_y & -3v_x & 0 & 0 & 0 & 0 & -3v_y & 3v_x & 0 \\
0 & -3v_z & 3v_y & 4S_{xx} & -2S_{xy} & -2S_{xz} & 0 & -3v_z & 3v_y & -2S_{xx} & S_{xy} & S_{xz} \\
3v_z & 0 & -3v_x & -2S_{xy} & 4S_{yy} & -2S_{yz} & 3v_z & 0 & -3v_x & S_{xy} & -2S_{yy} & S_{yz} \\
-3v_y & 3v_x & 0 & -2S_{xz} & -2S_{yz} & 4S_{zz} & -3v_y & 3v_x & 0 & S_{xz} & S_{yz} & -2S_{zz} \\
0 & 0 & 0 & 0 & 3v_z & -3v_y & 0 & 0 & 0 & 0 & -3v_z & 3v_y \\
0 & 0 & 0 & -3v_z & 0 & 3v_x & 0 & 0 & 0 & 3v_z & 0 & -3v_x \\
0 & 0 & 0 & 3v_y & -3v_x & 0 & 0 & 0 & 0 & -3v_y & 3v_x & 0 \\
0 & 3v_z & -3v_y & -2S_{xx} & S_{xy} & S_{xy} & 0 & 3v_z & -3v_y & 4S_{xx} & -2S_{xy} & -2S_{xz} \\
-3v_z & 0 & 3v_x & S_{xy} & -2S_{yy} & S_{yz} & -3v_z & 0 & 3v_x & -2S_{xy} & 4S_{yy} & -2S_{yz} \\
3v_y & -3v_x & 0 & S_{xz} & S_{yz} & -2S_{zz} & 3v_y & -3v_x & 0 & -2S_{xz} & -2S_{yz} & 4S_{zz}
\end{bmatrix}$$

$$+\frac{m}{A}\begin{bmatrix} \mathbf{0}_{3\times3} & \mathbf{0}_{3\times3} & \mathbf{0}_{3\times6} \\ \mathbf{0}_{3\times3} & \dot{\mathbf{R}}\bar{\mathbf{D}}_A\mathbf{R}^T + \mathbf{R}\bar{\mathbf{D}}_A\dot{\mathbf{R}}^T & \mathbf{0}_{3\times6} \\ \mathbf{0}_{6\times3} & \mathbf{0}_{6\times3} & \mathbf{0}_{6\times6} \end{bmatrix}$$

where $v_x = \dfrac{dl_x}{dt}$, $v_y = \dfrac{dl_y}{dt}$, $v_z = \dfrac{dl_z}{dt}$, $S_{xx} = l_y v_y + l_z v_z$, $S_{yy} = l_x v_x + l_z v_z$, $S_{zz} = l_x v_x + l_y v_y$, $S_{xy} = l_x v_y + l_y v_x$, $S_{xz} = l_x v_z + l_z v_x$, and $S_{yz} = l_y v_z + l_z v_y$.

(c) The expression for $\mathbf{H}^e$

$$\mathbf{H}^e = \begin{bmatrix} -\left(\dot{U}_5^2 + \dot{U}_6^2\right) & \dot{U}_4\dot{U}_5 & \dot{U}_4\dot{U}_6 & 0 & 0 & 0 & \left(\dot{U}_5^2 + \dot{U}_6^2\right) & -\dot{U}_4\dot{U}_5 & -\dot{U}_4\dot{U}_6 & 0 & 0 & 0 \\ \dot{U}_4\dot{U}_5 & -\left(\dot{U}_4^2 + \dot{U}_6^2\right) & \dot{U}_5\dot{U}_6 & 0 & 0 & 0 & -\dot{U}_4\dot{U}_5 & \left(\dot{U}_4^2 + \dot{U}_6^2\right) & -\dot{U}_5\dot{U}_6 & 0 & 0 & 0 \\ \dot{U}_4\dot{U}_6 & \dot{U}_5\dot{U}_6 & -\left(\dot{U}_4^2 + \dot{U}_5^2\right) & 0 & 0 & 0 & -\dot{U}_4\dot{U}_6 & -\dot{U}_5\dot{U}_6 & \left(\dot{U}_4^2 + \dot{U}_5^2\right) & 0 & 0 & 0 \\ 0 & 0 & 0 & 0 & 0 & 0 & 0 & 0 & 0 & 0 & 0 & 0 \\ 0 & 0 & 0 & 0 & 0 & 0 & 0 & 0 & 0 & 0 & 0 & 0 \\ 0 & 0 & 0 & 0 & 0 & 0 & 0 & 0 & 0 & 0 & 0 & 0 \\ \left(\dot{U}_5^2 + \dot{U}_6^2\right) & -\dot{U}_4\dot{U}_5 & -\dot{U}_4\dot{U}_6 & 0 & 0 & 0 & -\left(\dot{U}_5^2 + \dot{U}_6^2\right) & \dot{U}_4\dot{U}_5 & \dot{U}_4\dot{U}_6 & 0 & 0 & 0 \\ -\dot{U}_4\dot{U}_5 & \left(\dot{U}_4^2 + \dot{U}_6^2\right) & -\dot{U}_5\dot{U}_6 & 0 & 0 & 0 & \dot{U}_4\dot{U}_5 & -\left(\dot{U}_4^2 + \dot{U}_6^2\right) & \dot{U}_5\dot{U}_6 & 0 & 0 & 0 \\ -\dot{U}_4\dot{U}_6 & -\dot{U}_5\dot{U}_6 & \left(\dot{U}_4^2 + \dot{U}_5^2\right) & 0 & 0 & 0 & \dot{U}_4\dot{U}_6 & \dot{U}_5\dot{U}_6 & -\left(\dot{U}_4^2 + \dot{U}_5^2\right) & 0 & 0 & 0 \\ 0 & 0 & 0 & 0 & 0 & 0 & 0 & 0 & 0 & 0 & 0 & 0 \\ 0 & 0 & 0 & 0 & 0 & 0 & 0 & 0 & 0 & 0 & 0 & 0 \\ 0 & 0 & 0 & 0 & 0 & 0 & 0 & 0 & 0 & 0 & 0 & 0 \end{bmatrix}$$

(d) Dynamic Equivalence

The requirements for dynamic equivalence are [19]:
1- The mass of the equivalent body must equal to the original body

$$m = m_1 + m_{p_o} + m_{p_1} \tag{A.1}$$

2- The centre of gravity of the equivalent body must be in the same location of the original body.

$$m\, l_c = m_1 \frac{l}{2} + m_{p_1} l \tag{A.2}$$

3- The mass moment of inertia of the equivalent body must equal that of the original body.

$$I_{A_x} = I_x \tag{A.3}$$

$$m_1 \left[\frac{l^2}{12} + \left(\frac{l}{2} - l_c\right)^2\right] + m_{p_o} l_c^2 + m_{p_1}\left(l - l_c\right)^2 + I_{A_y} = I_y \tag{A.4}$$

$$m_1 \left[\frac{l^2}{12} + \left(\frac{l}{2} - l_c\right)^2\right] + m_{p_o} l_c^2 + m_{p_1}\left(l - l_c\right)^2 + I_{A_Z} = I_z \tag{A.5}$$

Since I_{A_x} , I_{A_y} , and I_{A_z} depend on the cross sectional area of the link not its length, see Fig. 6, then

$$I_{A_x} = I_{A_y} + I_{A_z} \tag{A.6}$$

The solution of the above six linear equations gives the parameters required for the homogeneous equivalent link $\left\{m_1, m_{p_o}, m_{p_1}, I_{A_x}, I_{A_y}, I_{A_z}\right\}$.

2/25/2018